ELECTROSTATIC PARTICLE BASED MODELING AND SIMULATION OF ULTRA COLD PLASMA

By

Mayur Jain

A THESIS

Submitted to
Michigan State University
in partial fulfillment of the requirements
for the degree of

Electrical Engineering - Master of Science

2015

ABSTRACT

ELECTROSTATIC PARTICLE BASED MODELING AND SIMULATION OF ULTRA COLD PLASMA

By

Mayur Jain

We model moderately coupled ultra cold plasma based on experimental setups and investigate the influence of external electric and magnetic fields by simulating the interaction of this plasma with constant magnetic field and radio frequency electric fields in the form of continuous application and short pulses. A density dependent resonant response is observed through these simulations and we infer the cause to be rapid energy transfer to individual electrons from electric fields through the collective motion of the electron cloud rather than a collision based mechanism since collisional time scales are found to be larger than the response period. It is also observed that electron evaporation influences the UCP expansion by reducing the electron temperature significantly. These arguments are corroborated by experimental results. We report diagnostics such as temperature, potential and density evolution, electron and ion pair correlation functions, and estimate the size of the UCP with varying initial ionization energies for the ultra cold plasma throughout complete simulation.

ACKNOWLEDGMENTS

This work would not have been possible without my advisors Dr. John Verboncoeur and Dr. Andrew Christlieb who have been excellent mentors and granted me this great opportunity to work on an exciting research project. I am immensely grateful to both of them for their guidance throughout the completion of my work. I would also like to thank my committee member Dr. Prem Chahal for his valuable suggestions and comments on my work.

I would like to express my appreciation to my fellow graduate students, Gautham Dharuman for his intellectual discussions and constant support and Guy Parsey for all the technical help he has offered me. I thank them and everybody in the group for creating a very healthy research environment.

Finally, I would like to thank my family for believing in me and encouraging me with all their love and motivation.

TABLE OF CONTENTS

LIST OF FIGURES

Chapter 1

Introduction

Ultracold neutral plasma were produced by rapidly photo-ionizing small laser cooled clouds of atoms. These novel plasma present interesting theoretical challenges. This work focuses on the development of new modeling and simulation tools for studying strongly coupled plasma as they differ from traditional plasma in that the potential energy is larger than the kinetic energy. These include dusty ionospheric plasma, plasma from ultra-fast lasers/materials interactions, plasma generated by conventional explosives, molecular plasma for chemical investigation, and even exotic warm dense matter found in high energy density and astrophysical contexts. For example, consider the case of dust in the ionosphere. In the ionosphere, dust particles are typically 100 to 1000 times more massive than the typical ions. The light mobile electrons impact the non-conducting dust, which charges up negatively. On average, the dielectric dust carries orders of magnitude more charge than the charge of a background ion. With a high enough density of dust, the heavy immobile dust forms a lattice of strongly interacting bound charge that has the effect of modifying the permittivity of the plasma. A standard quasi neutral plasma approximation is inadequate in this case. In addition to the possibility of quantum effects, the standard quasi neutral plasma model does not account for two major effects: change in the permittivity for modeling EM waves and impact on relaxation of charged particles undergoing Coulomb collisions in a system with weakly shielded long range interactions. The unique aspect of strongly coupled plasma (SCP) is that the potential energy exceeds the kinetic energy. Strong coupling is defined in

terms of the dimensionless parameter, often referred to as the Coulomb coupling parameter,

$$\Gamma = \frac{(Ze)^2}{kTa} \tag{1.1}$$

which is the ratio of the potential energy to kinetic energy. In the above expression; Z is the charge number of the ion species, e is the unit charge, k is Boltzmann's constant, T is the temperature of the species in Kelvin, $a = [3/(4\pi n)]^{1/3}$ is the Wigner-Seitz radius (mean inter-particle distance), and n is the density of the species. Coupling parameter Γ effectively defines correlation. When $\Gamma << 1$, the charged species in the plasma has no long range correlation and binary collisions characterize Coulomb scattering for that species. For $\Gamma \sim 1$, the plasma species in question begins to exhibit long range correlation. As Γ increases in these systems, the plasma exhibits a collective behavior, giving the system properties resembling liquids and solids. Collective oscillations are a fundamental feature of ultra cold plasma (UCP) and help determine it's response to an external perturbation. For a uniform density plasma, if the thermal motion of electrons is ignored, the plasma frequency is expressed as $\omega_p = \sqrt{e^2 n_e / m_e \epsilon_0}$, where e is the electric charge, m_e is the effective mass of the electron, n_e is the charge density and ϵ_0 is the free space permittivity. Since UCP cannot be considered to have uniform densities, the resonant frequency condition is not applicable directly, however, it's resonant response to RF fields is a subject of experimental and theoretical work. UCP expansion rates could be measured through application of an external RF field since plasma oscillations are density dependent. Here, we explore this density dependent resonant response by applying RF fields continuously and in short bursts. Our focus in this work is on the collective motion of the electrons in these resonant responses.

Chapter 2

Boundary Integral Treecode

The grid-free Lagrangian approach starts by casting Poisson's equation in integral form,

$$\phi(\mathbf{y}) = \int_{\Omega} G(\mathbf{x}|\mathbf{y}) \frac{\rho(\mathbf{x})}{\varepsilon_0}\, d^3\mathbf{x} + \oint_{\partial\Omega} \left[(\phi(\mathbf{x}) \bigtriangledown_{\mathbf{x}} G(\mathbf{x}|\mathbf{y}) - G(\mathbf{x}|\mathbf{y}) \bigtriangledown_{\mathbf{x}} \phi(\mathbf{x})) \right] . \widehat{\mathbf{n}}\, dS_{\mathbf{x}} \qquad (2.1)$$

where $\mathbf{y} \in \Omega \setminus \partial\Omega$ and $G(\mathbf{x}|\mathbf{y})$ is the free space Green's function. Note that the volume integral is the particular solution, $\phi_P(\mathbf{y})$, of Poisson's equation and the boundary integral is the homogeneous solution, $\phi_H(\mathbf{y})$, i.e., $\phi(\mathbf{y}) = \phi_P(\mathbf{y}) + \phi_H(\mathbf{y})$. Depending on the boundary conditions, $\phi_H(\mathbf{y})$ can be either modeled as

$$\phi_H = \oint_{\partial\Omega} \alpha(\mathbf{x}) G(\mathbf{x}|\mathbf{z})\, dS_{\mathbf{x}} \quad or \quad \phi_H = \oint_{\partial\Omega} \beta(\mathbf{x}) \partial_n G(\mathbf{x}|\mathbf{z})\, dS_{\mathbf{x}} \qquad (2.2)$$

which is a single layer or double layer potential respectively and $\alpha(\mathbf{x})$ and $\beta(\mathbf{x})$ are the unknown dipole strengths that can be determined by solving an integral equation for the Poisson's equation on the boundary or surface. Imposing consistency, and appropriately handling the singularity of $\partial_n G$ on the boundary, we use the above boundary integral for ϕ_H to numerically correct the particular solution. The Vlasov equation written in a Lagrangian reference frame transforms the model into an evolution equation which describes

the dynamics of phase space contours,

$$\begin{aligned}
\dot{\mathbf{x}}^k &= \mathbf{v}^k \\
\dot{\mathbf{v}}^k &= \bigtriangledown\phi_P(\mathbf{x}^k) + \bigtriangledown\phi_H(\mathbf{x}^k) \\
\phi_P(\mathbf{x}^k) &= \sum_{l\in\pm} \frac{q^l}{\epsilon_0}\Big(\int\int_{\Gamma_t^l} G(\mathbf{x}^l|\mathbf{x}^k) f^l(t,\mathbf{x}^l,\mathbf{v}^l)\, d\mathbf{x}^l d\mathbf{v}^l\Big)
\end{aligned}$$

where $(\mathbf{x}^k, \mathbf{v}^k)$ is the flow map for the phase space contours of species k, the sum is over l species and Γ_t^l is the phase space volume at time t. Each point in the flow is a function of its initial phase space point, $\mathbf{x}^k = \mathbf{x}^k(t, \mathbf{x}_o^k, \mathbf{v}_o^k)$ and $\mathbf{v}^k = \mathbf{v}^k(t, \mathbf{x}_o^k, \mathbf{v}_o^k)$. Since the solutions of this system are volume preserving, it is easy to show that under a change of variables, $\Gamma_t \to \Gamma_{t0}$, where Γ_{t0} is the initial phase space volume, the following holds,

$$f^l(t, \mathbf{x}^l(t, \mathbf{x}_o^l, \mathbf{v}_o^l), \mathbf{x}^l(t, \mathbf{x}_o^l, \mathbf{v}_o^l))|J(\mathbf{x}^l, \mathbf{v}^l)| = f^l(t, \mathbf{x}_o^l, \mathbf{v}_o^l) \tag{2.3}$$

where $J(\mathbf{x}^l, \mathbf{v}^l)$ is the Jacobian. Given this identity, the Lagrangian flow map may be written as,

$$\begin{aligned}
\dot{\mathbf{x}}^k(t, \mathbf{x}_o^k, \mathbf{v}_o^k) &= \mathbf{v}^k(t, \mathbf{x}_o^k, \mathbf{v}_o^k) \\
\dot{\mathbf{v}}^k(t, \mathbf{x}_o^k, \mathbf{v}_o^k) &= \bigtriangledown\phi_P(\mathbf{x}^k(t, \mathbf{x}_o^k, \mathbf{v}_o^k)) + \phi_H(\mathbf{x}^k(t, \mathbf{x}_o^k, \mathbf{v}_o^k))
\end{aligned} \tag{2.4}$$

$$\phi_P(\mathbf{x}^k(t, \mathbf{x}_o^k, \mathbf{v}_o^k)) = \sum_l \frac{q^l}{\epsilon_0} \int\int_{\Gamma_{t0}^l} G(\mathbf{x}^l(t, \mathbf{x}_o^l, \mathbf{v}_o^l)|(\mathbf{x}^k(t, \mathbf{x}_o^k, \mathbf{v}_o^k)) f^l(t_0, \mathbf{x}_o^l, \mathbf{v}_o^l) d\mathbf{x}_0^l d\mathbf{v}_0^l \tag{2.5}$$

Choosing $N = N_+ + N_-$collocation points and applying systematic collocation to Eq. (2.5) gives rise to a system of N coupled ODE which describe the discrete flow map. Eq. (2.5)

takes the form,

$$\phi_P(\mathbf{y}) = -\sum_{j=1}^{N_+} \frac{q_+ w_j}{\epsilon_0} G(\mathbf{x}_j|\mathbf{y}) + \sum_{k=1}^{N_-} \frac{q_- w_k}{\epsilon_0} G(\mathbf{x}_k|\mathbf{y}) \tag{2.6}$$

where $w_{j,k}$ are quadrature weights determined at t_0

2.1 Treecode algorithm

Evaluating the sum in Eq.(2.6) is an N-body problem and the CPU time is an important issue. A treecode algorithm is employed to reduce the operation count from $O(N^2)$ to $O(NlogN)$. In this algorithm, the particles are divided into a hierarchy of clusters and the particle-particle interactions are replaced by particle-cluster interactions which are evaluated using multipole expansions. The Barnes-Hut treecode cleverly groups nearby bodies and recursively divides sets of bodies storing them in trees (Fig. 2.1). The topmost node represents the whole space while the children form quadrants of space. Particles are spatially divided based on their physical locations. Each external node represents a single body while each internal node represents the group of bodies beneath it, and stores the center-of-mass and the total mass of all its children bodies. Barnes and Hut used monopole approximations and a divide-and-conquer evaluation strategy. Treecode algorithms have been very successful in particle simulations and there is ongoing interest in optimizing their performance.

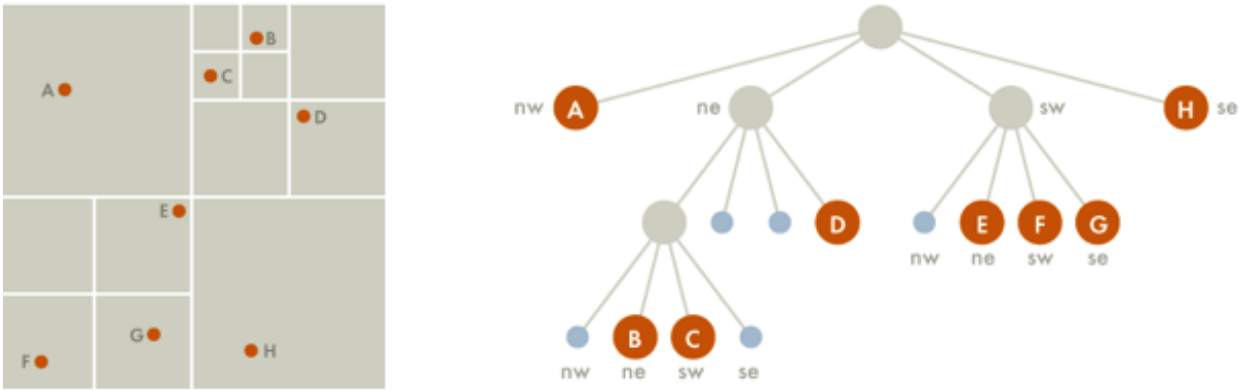

Figure 2.1: Structure of a sample parent quadtree with children nodes. Empty quadrants are possible.

Fig. adapted from The Barnes-Hut Algorithm, Tom Ventimiglia and Kevin Wayne

2.2 Point-cluster interactions

The potential $\phi_P(\mathbf{y})$ is first expressed as

$$\phi_P(\mathbf{y}) = \sum_{C_r} \sum_{j \in C_r} w_j G(\mathbf{x}_j|\mathbf{y}) = \sum_{C_r} \phi_i(\mathbf{y}, C_r)$$

$$\phi_i(\mathbf{y}, C_r) = \sum_{j \in C_r} w_j G(\mathbf{x}_j|\mathbf{y}) \tag{2.7}$$

where $C_r = \{\mathbf{x}_j | \mathbf{x}_j \in C_r \text{ and } \mathbf{x}_j \notin \{\cup_s C_s \setminus C_r\}\}$ denotes a cluster of particles and $\phi_i(\mathbf{y}, C_r)$ is the potential at point $\mathbf{y}$ due to cluster C_r. The procedure for choosing the clusters will be explained below; for now it is enough to assume clusters in Eq. (2.7) are non-overlapping and their union is the whole distribution. To calculate the net force on a particular body, traverse the nodes of the tree, starting from the root (Fig. 2.2). If the center-of-mass of an internal node is sufficiently far from the body, approximate the bodies contained in that part of the tree as a single body, whose position is the group's center of mass and whose mass is the group's total mass. The algorithm is fast because we don't need to individually

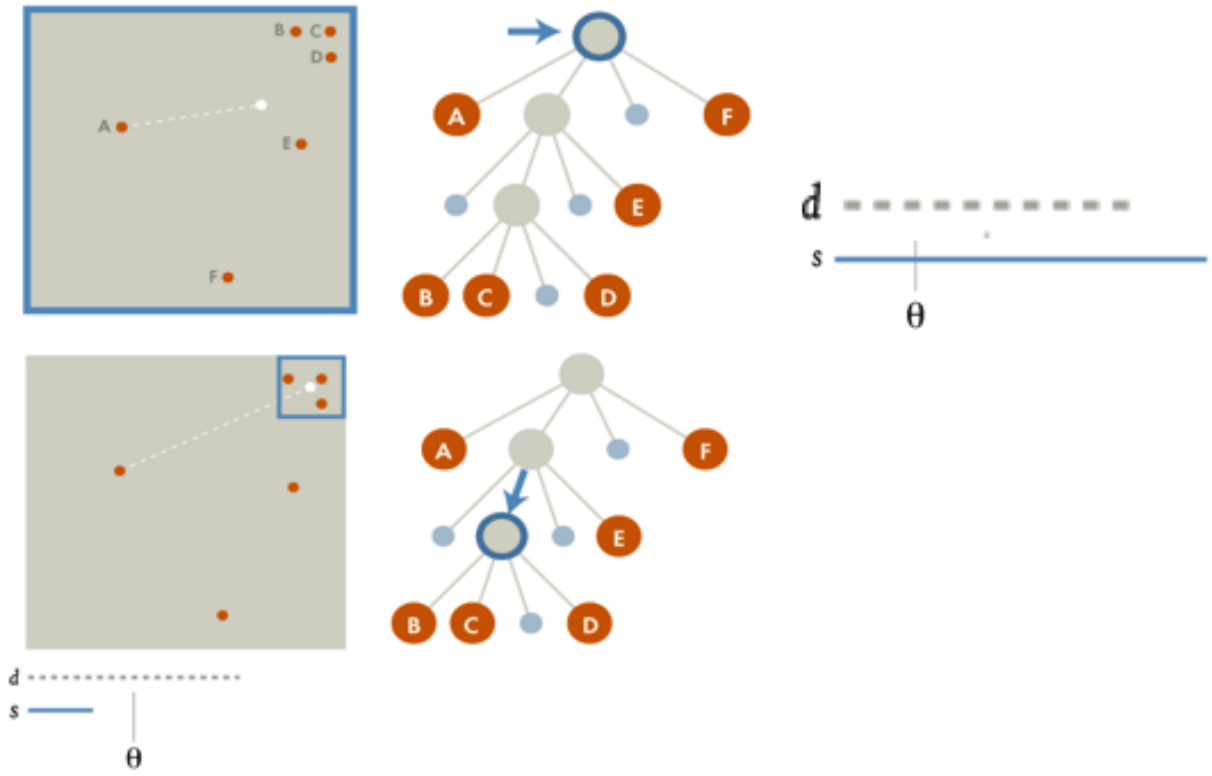

Figure 2.2: Illustration of node traversal for cluster monopole approximation.

Fig. adapted from The Barnes-Hut Algorithm, Tom Ventimiglia and Kevin Wayne

examine any of the bodies in the group. If the internal node is not sufficiently far from the body, recursively traverse each of its subtrees. To determine if a node is sufficiently far away, compute the quotient s/d, where s is the width of the region represented by the internal node, and d is the distance between the body and the node's center-of-mass. Then, compare this ratio against a threshold value θ. If $s/d < \theta$, then the internal node is sufficiently far away. By adjusting the θ parameter, we can change the speed and accuracy of the simulation. We always use $\theta = 0.5$, a value commonly used in practice. Note that if $\theta = 0$, then no internal node is treated as a single body, and the algorithm degenerates to brute force.

Performing a Taylor expansion of the Green's function about the cluster center x_{cr},

$$\begin{aligned}\phi_i(\mathbf{y}, C_r) &\approx \sum_{j \in C_r} \sum_{l=0}^{p} \frac{1}{l!} \partial_{\mathbf{y}}^l G(\mathbf{x}_{cr}|\mathbf{y}) \big(w_j (\mathbf{x}_j - \mathbf{x}_c)^l\big) \\ &= \sum_{l=0}^{p} \frac{1}{l!} \partial_{\mathbf{x}}^l G(\mathbf{x}_{cr}|\mathbf{y}) \sum_{j \in C_r} w_j (\mathbf{x}_j - \mathbf{x}_c r)^l \\ &= \sum_{l=0}^{p} T_l(\mathbf{x}_{cr}, \mathbf{y}) M_l(C_r) \end{aligned} \tag{2.8}$$

where p is the order of approximation, $T_l(\mathbf{x}_{cr}, \mathbf{y})$ is the l^{th} Taylor coefficient of the Green's function, and $M_l(C)$ is the l^{th} moment of the cluster. Note that Cartesian multi-index notation is being used. The speedup occurs because the cluster moments are independent of the point $\mathbf{y}$, while the $T_l(\mathbf{x}_{cr}, y)$ are independent of the number of particles in C_r. This form of the fast summation is suited to a regularized kernel. The C_r have a hierarchical tree structure. Typically, C_r on each level of the tree are uniform cubes obtained by bisecting the previous generation of clusters in each coordinate direction. The potential ϕ_i is evaluated using the tree structure in a recursive divide-and-conquer strategy.

We examine the error for the treecode in comparison with direct summation (Figure 2.3) for the problem of computing potential V for a test case of randomly distributed particles inside a cube. The set of representative parameter values used for the treecode were $\theta = 0.5$ for the multipole acceptance criterion (MAC), $p = 1 : 5$ for order of Taylor approximation and maximum number of particles in the leaf $N_{leaf} = 100$.

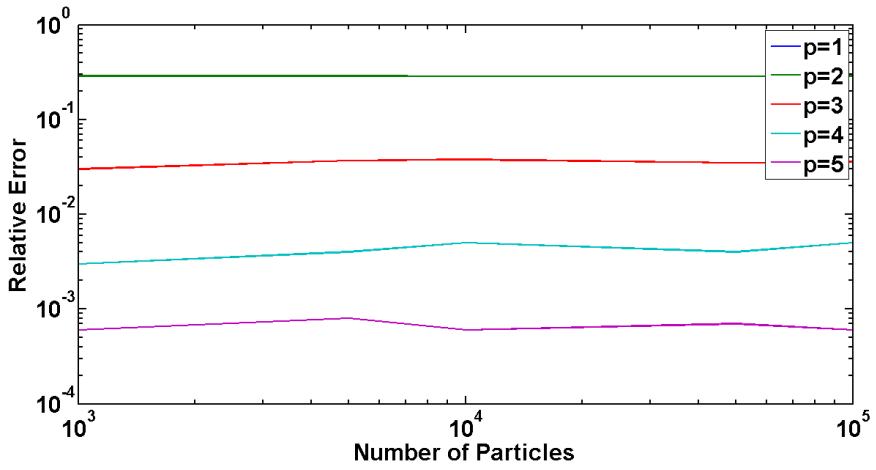

Figure 2.3: Relative error on potential varying with multipole order for randomly distributed particles inside a cube

Figure 2.4 shows the CPU time as a function of the number of particles N and the approximation of order p. The CPU time is $O(N^2)$ for direct summation and is consistent with $O(NlogN)$ for the treecode. For a smaller number of particles ($< 10^3$) and $\theta = 0.5$, most particle - cluster interactions are computed by direct summation and since relatively very few Taylor approximations are evaluated, the overhead increases. However, with a sufficiently large number of particles N, the treecode outperforms direct summation.

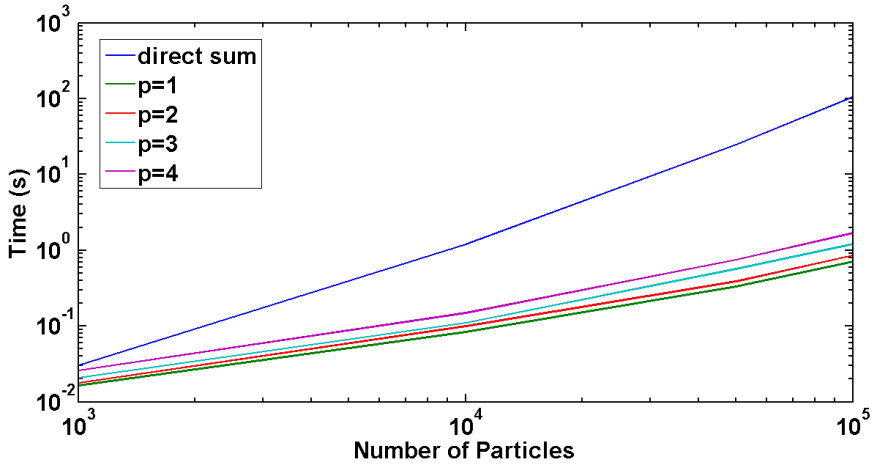

Figure 2.4: Timing comparison for treecode with varying multipole order vs. direct summation for randomly distributed particles inside a cube

2.3 Regularizing the kernel

It is important to note that in 2D and 3D, the electrostatic force, $\mathbf{F}_j$ (the gradient of Eq. (2.1)), becomes singular as the distance between the particles tends to zero. When we discretize the Lagrangian form of the Vlasov equation, time stepping particles may cause two particles to approach closer than their minimum separation in the continuous case. Accuracy constraints imposed to avoid this issue can place a severe restriction on the maximum allowable time step. Our approach to overcoming this problem is to regularize the Green's function, i.e. in three dimensions use

$$G_{3D}^{d}(\mathbf{x}|\mathbf{y}) = -\frac{1}{4\pi(\|\mathbf{x}-\mathbf{y}\|_2^2 + d^2)}$$

where d is a parameter, so that the maximal force in 3D is proportional to $1/d^2$. In 1D, this issue arises when two test particles cross, since the force in 1D has a discontinuity. Hence, to achieve high order with explicit time stepping, even the 1D Green's function must be regularized.

Chapter 3

Simulation Parameters

The number of parameters that define our simulations is reduced to a minimum by using length scaled by the Wigner-Seitz radius, a and time, ω_p^{-1}. With this, the equations of motion and initial conditions are specified by : mass ratio m_i/m_e, electron density n_e, coupling parameter Γ_e and the Coulomb potential regularization parameter ϵ.

3.1 Initial conditions

The mass ratio m_i/m_e is taken as 100 to ensure ions have time to participate in the simulation dynamics. The initial number of electrons and ions in our system is on the order of $\sim 10^5$, and we arrange the boundary conditions to start with a uniform spherical Gaussian electron-ion density distribution described by $n(r) = n_0\, exp(-r^2/2\sigma^2)$ (Fig. 3.1), where n_0 is the peak density and σ characterizes the spatial extent of the strongly coupled ultra cold plasma. These plasma typically has a peak plasma density of $n_i = n_e = 10^{13} - 10^{14}\,\mathrm{m}^{-3}$ which is about an order or two lower than most UCP experiments and $\sigma \sim 1\,\mathrm{mm}$. We first begin with $T_e \simeq 1\,\mathrm{K}$ and $T_i \simeq 10\,\mu\mathrm{K}$. The electron-electron self equilibration time in this case is more than $1\,\mu\mathrm{s}$. An external electric field ($\sim 2 - 8\,\mathrm{V/m}$) is applied to pull the escaping electrons with the assistance of a guiding magnetic field ($\sim 7 - 9\,\mathrm{G}$) which is axially symmetric with respect to the electrodes.

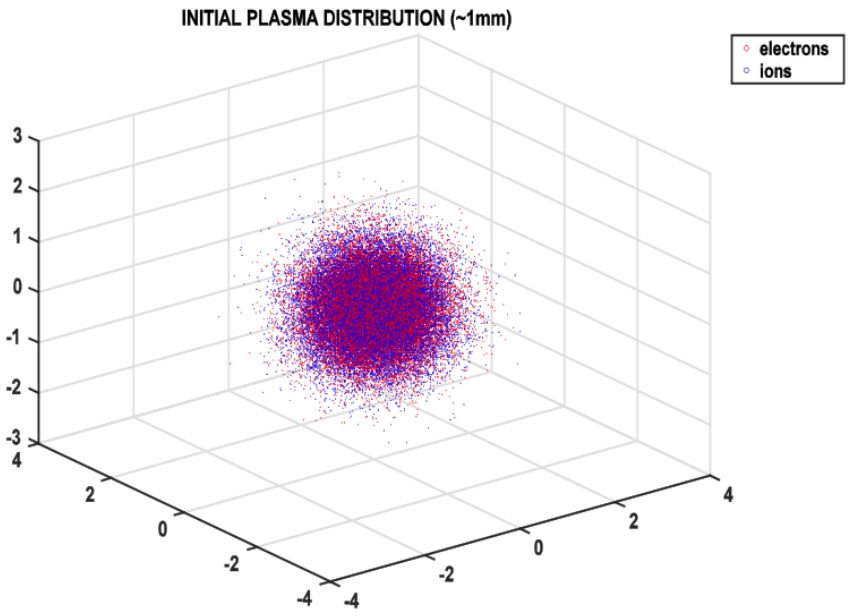

Figure 3.1: Initial plasma distribution

3.2 Early evolution of the UCP

We obtain a histogram of electron kinetic energies and match them to a Maxwellian. Rapid heating initially raises $\Gamma \simeq 1$. The longer term slower heating maybe associated with three body recombination.

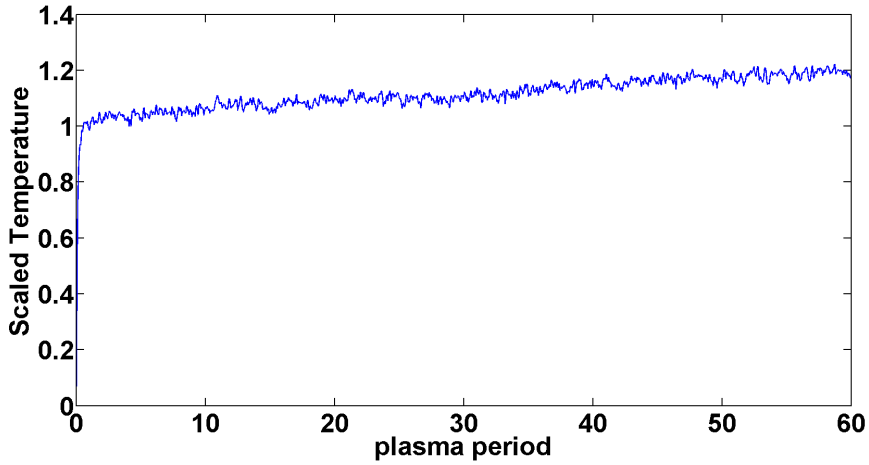

Figure 3.2: Scaled temperature vs scaled time displaying kinetic energy oscillation

The electron-electron pair correlation function is time averaged over about $t\omega_p = 3$ *to* 7 and the correlation function starts out flat corresponding to randomly distributed electrons and relaxes at a later stage.

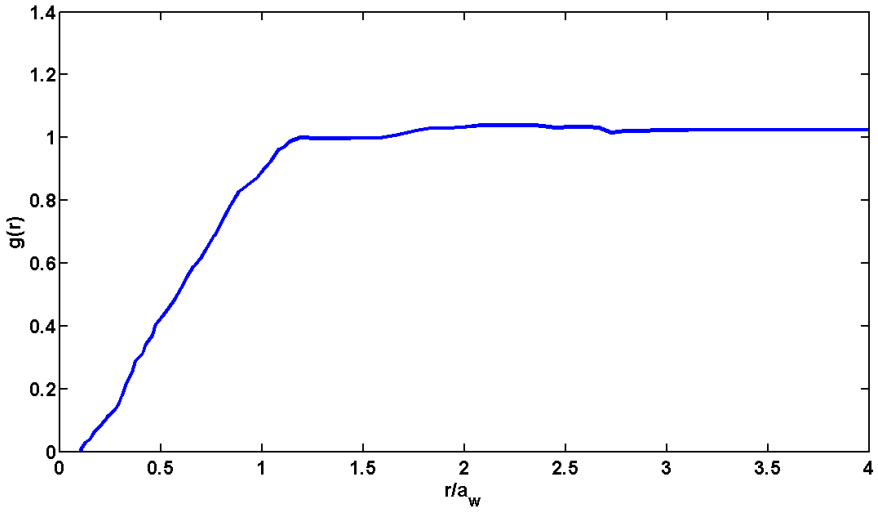

Figure 3.3: Electron pair correlation function for early evolution corresponding to $\Gamma \simeq 1$

The ion-ion correlation funtion behaves in a very similar fashion except that it is averaged over $t\omega_p = 65$ *to* 70 as the relaxation time is longer than that for the electrons. The coupling here is about $\Gamma \sim 1$

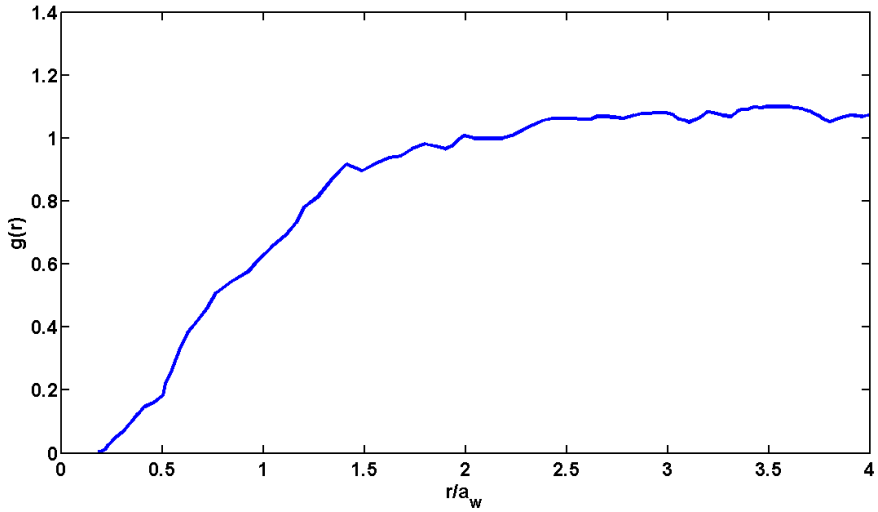

Figure 3.4: Ion pair correlation function for early evolution corresponding to $\Gamma \simeq 1$

From these simulation results, we see that intrinsic rapid heating prevents development of a strong correlation even when initial electron and ion temperatures are $0\ i.e, \Gamma_e(0) = \Gamma_i(0) \sim \infty$. Electron evaporation from an unbounded cloud, being a cooling mechanism also does not compete with the heating. Although these simulations only follow early evolution and plasma expansion at a later stage can be a strong cooling mechanism that could reduce the temperature of the plasma. Low initial temperatures do not directly lead to strong correlation during early times.

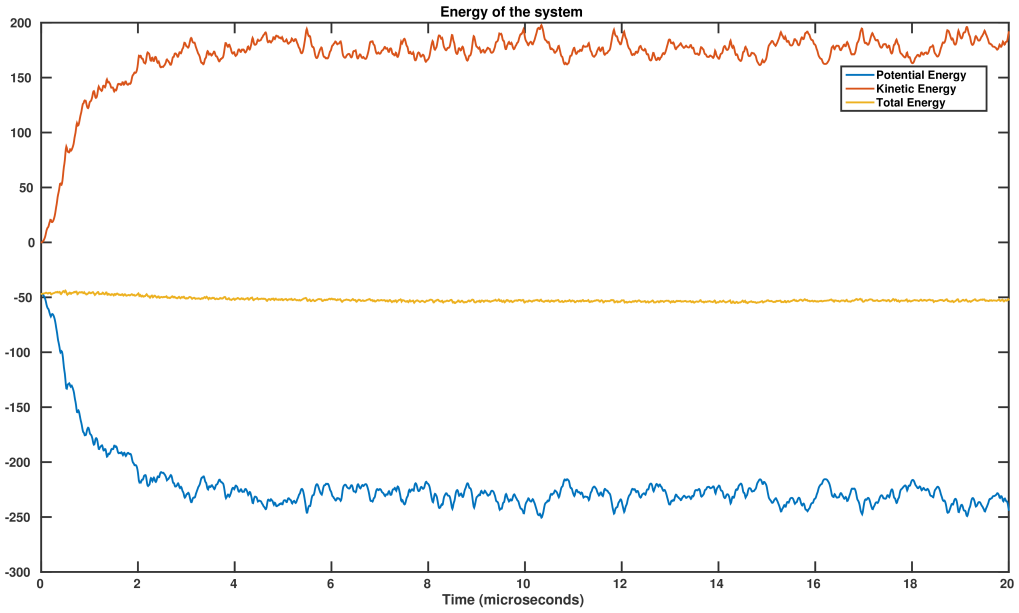

Figure 3.5: System energy in K for complete simulation displaying Coulomb potential energy is greater than kinetic energy and confirming conservation of the total energy

Chapter 4

Results

All simulations in this work are obtained for a one to one physical representation of the charged species. Velocity for the species is sampled from a Maxwell-Boltzmann distribution. The random numbers used for our simulations are generated with the srand pseudo random number generator which is seeded with the system time. Time integrator for equations of motion is fourth order Runge-Kutta method. Results shown in this section are smoothed by time averaging each point for over 1000 runs.

Collective oscillations are one of the fundamental features in an ultra cold plasma and can help characterize it's density as they freely expand. We apply external RF electric fields to excite the oscillations to measure the UCP expansion rate also allowing us to infer early time temperature and it's subsequent evolution. In this section, results from previous experimental UCP work are also discussed as a basis for comparison. We first look at the evolution of a neutral ultra cold plasma.

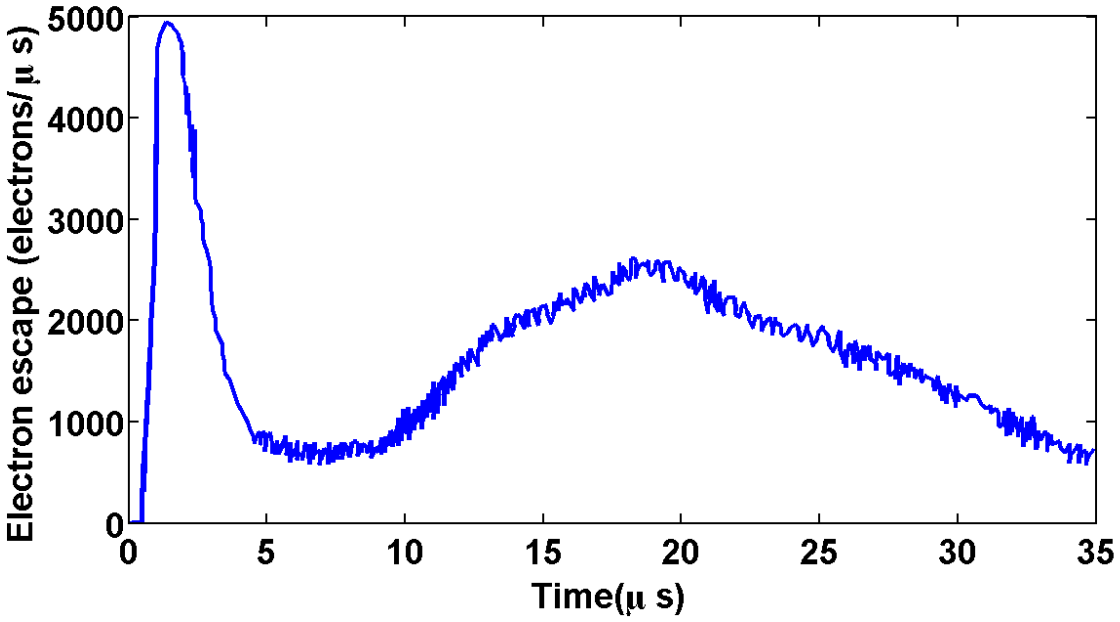

Figure 4.1: Typical electron escape signal from the ultra cold neutral plasma (1×10^5 electron-ion system)

Fig. 4.1 shows the plasma evolution and expansion process. We begin with an initially neutral ultra cold plasma and therefore we see a bunch of electrons escape at $t = 0$ due to the finite energy of electrons and no net confinement due to absence of external fields. The resulting excess positive charge creates a Coulomb potential well greater than the average electron temperature, trapping the remaining electrons. Electrons must have an energy higher than the initial formation energy to escape the UCP and electrons now begin to thermalize. This creates an energy distribution where only the highest energy electrons are able to escape the UCP lowering the overall temperature of electrons. Greater temperature of electrons compared to ions will cause the electron density to decrease in space slightly relative to the ions. This decrease in electron density produces electric fields that confine the electrons but now drive the ion expansion. As the UCP size increases, the potential well shallows allowing more electrons to escape.

4.1 Continuous RF response

Electrons from the ultracold plasma escape immediately directed by the external electric field since there is no net confinement, and produce the first peak in the signal resulting in an excess of positive charge in the plasma, thereby creating a Coulomb potential well which traps the remaining electrons. High energy electrons begin to escape the UCP.

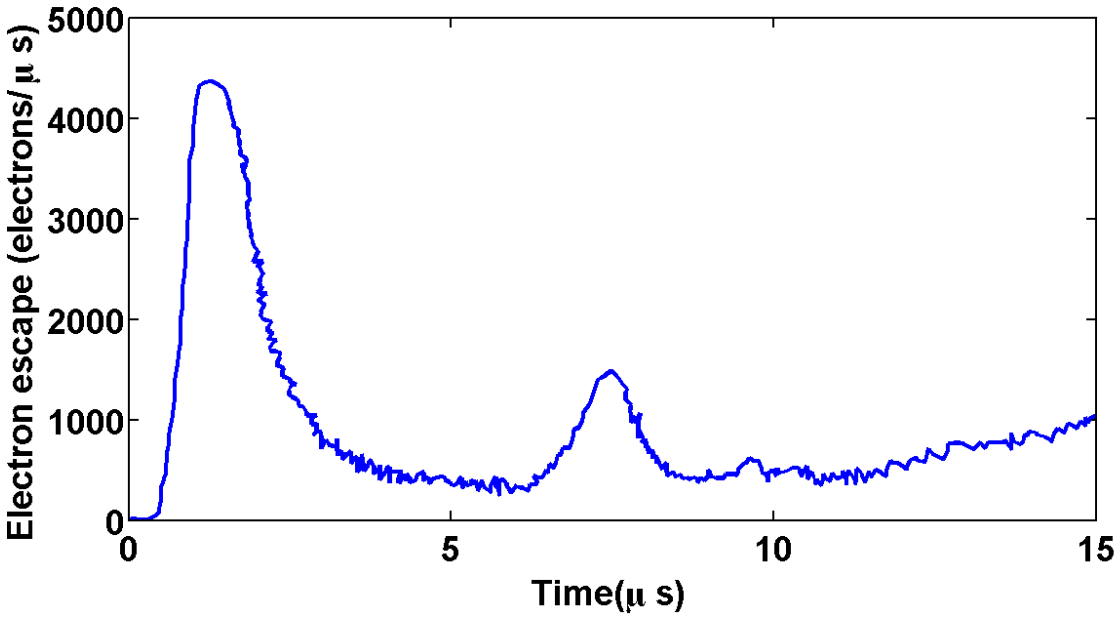

Figure 4.2: Plasma response ($\Delta E/k_B = 200K$, 1×10^5 electron-ion system, $6V_{p-p}/m$) with continuous RF application of $17MHz$

In the presence of an external RF field, in addition to the response as seen in Fig. 4.1, an additional peak appears in the electron escape signal (Fig. 4.2). The applied RF excites plasma oscillations at the resonant frequency as the UCP expands and decreases in density. The amplitude of these oscillations is much less than σ. Previous work implied that the acquired energy is collisionally redistributed but this does not occur instantaneously as the time scale is associated with the electron self-equilibration time, which scales with both density and temperature of the plasma and is approximately proportional to $T_e^{3/2}/n_e$. The escaping

electrons have a higher energy than the average electron energy, so the energy transfer would in fact be slower. It was also assumed that the applied RF was only resonant within regions of plasma where densities satisfy the resonance condition $f = (1/2\pi)\sqrt{e^2 n_e/m_e\epsilon_0}$ where f is the applied RF frequency. We observe collective oscillations to be the phenomenon.

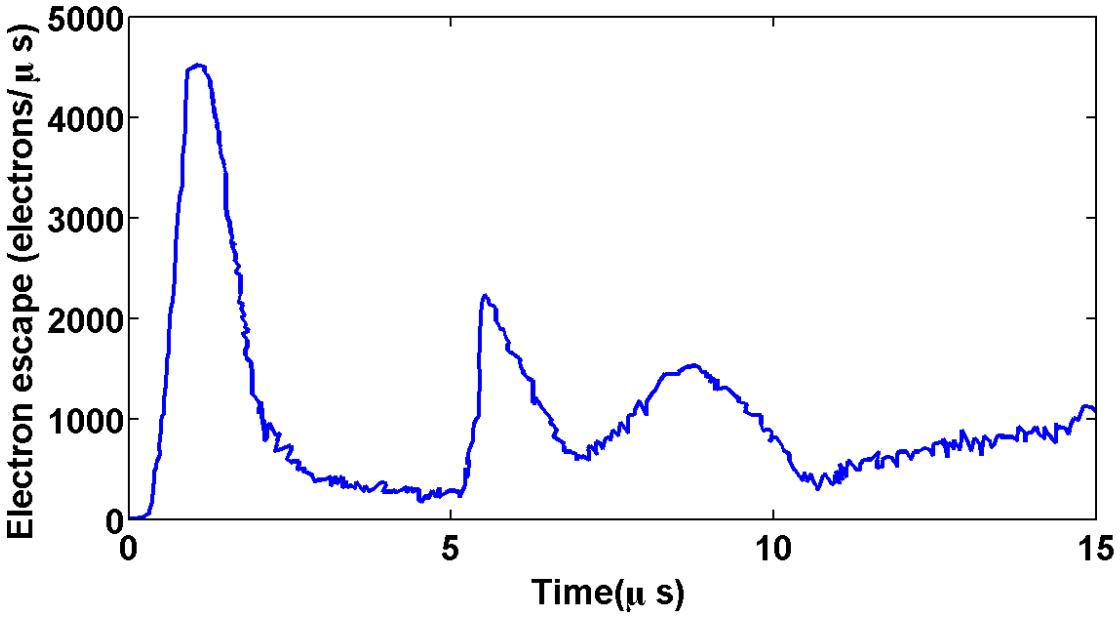

Figure 4.3: The plasma response ($\Delta E/k_B = 200K$, 1×10^5 electron-ion system, $6V_{p-p}/m$) with RF turned on at 5μ s (bottom) at an applied frequency of $\sim 17MHz$

We also apply RF near resonance at a particular time by delaying the application until after a certain point (5μs) (Fig. 4.3) in the plasma evolution and measure the time delay associated with the collisions, but this produces a rapid response of electron escape with no real dependence on temperature or density. The response time here is much shorter than the collisional time scale implying a different mechanism other than collisional redistribution of energy among the electrons. The resonant response is also shifted to later in time. The initial peaks may change in height as a function of the applied frequency. This rapid response can also be seen by exciting the plasma with a few cycles of RF pulses.

4.2 Response with RF pulses

We apply a two cycle pulse to the UCP, generating a peak in the response indicating resonance at the particular time for the applied frequency. Applying short bursts of RF pulses induces a density dependent resonant response with a short delay between the application and the response, indicating yet again that the model is based on collective motion of the electron cloud (Fig. 4.4) which produces internal electric fields and is the main mechanism for energy transfer causing individual electrons to escape the plasma.

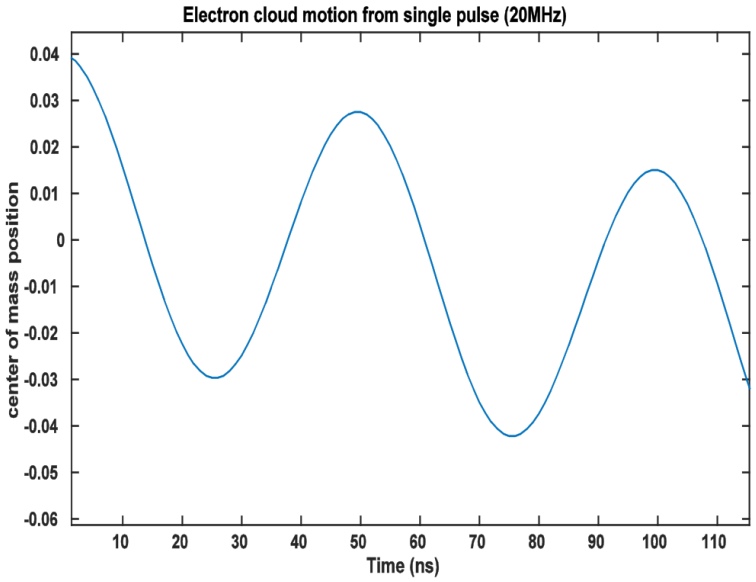

Figure 4.4: UCP electron cloud response ($\Delta E/k_B = 200K$, 5×10^5 electron-ion system, $8V_{p-p}/m$) with a single RF pulse $20MHz$

The two cycle response can be compared with the UCP response when no RF is applied to determine when the signal response occurs relative to the initial onset of the pulse. The peak in the response is observed at the resonant frequency achieved by successively changing through measurements.

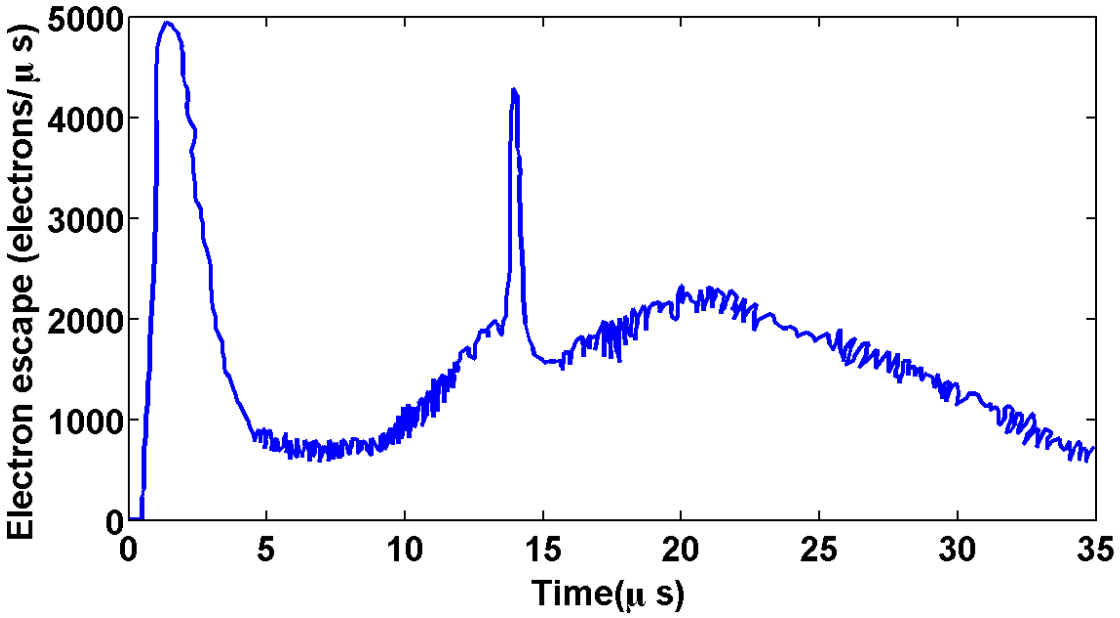

Figure 4.5: Plasma response to a $8V_{p-p}/m$, $20MHz$, 2 cycle RF signal applied to the 5×10^5 electron-ion system, $\Delta E/k_B = 200K$, showing a peak soon after the applied pulse

4.3 Diagnostics

Response of the UCP depends strongly on many parameters, density being only one of them. The nature of the responses with continuous application and pulses could be compared under similar conditions. The effect of delay in the RF application causes a shift in the resonance time, and responses with continuous RF application change with the amplitude of the field applied as the resonance shifts to an earlier time with an increased amplitude, implying heating of the UCP that drives a faster expansion.

We begin our simulations with a UCP density of about $10^7 cm^{-3}$ and as discussed earlier, electrons start escaping the plasma immediately and the plasma begins to expand. The applied RF drives electrons out of the system and the reduced electron density drives the plasma expansion due to the internal electric field it produces. All these factors contribute to

a reducing UCP density as shown below in figure 4.6. The average density can be described by

$$\bar{n} = N/[4\pi(\sigma_0^2 + v_0^2 t^2)]^{3/2} \tag{4.1}$$

where σ_0 is the initial rms radius, v_0 is the rms radial velocity that could equate to $v_0 = (k_B T_e/m_i)^{1/2}$. The UCP expansion can be related to the electron temperature as $\sigma(t)^2 = \sigma(0)^2 + (v_0 t)^2$. $\bar{n}$ is the density in resonance with the RF field assumed to be equal to the average density in plasma.

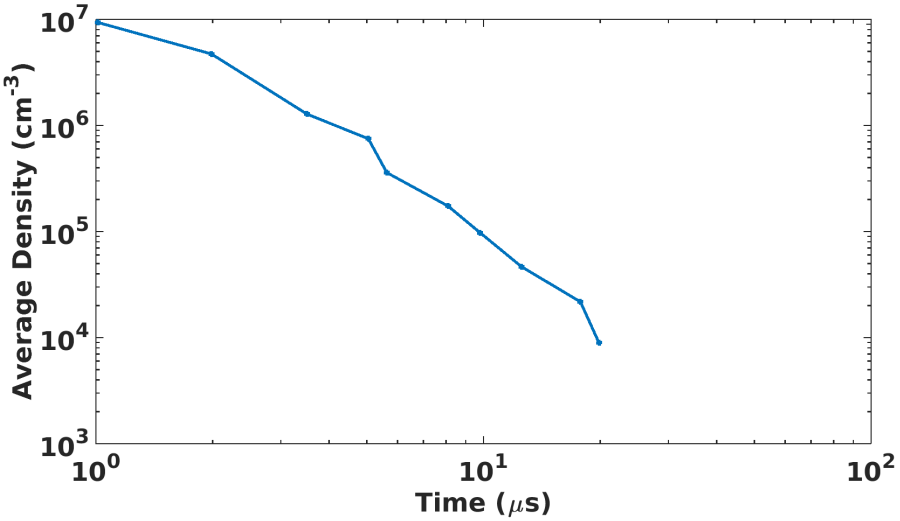

Figure 4.6: Desnity evolution indicating expansion of the plasma for $N = 5\times10^5$ electron-ion UCP system

The temperature of the UCP (Fig. 4.7), after an inital rise, drops steadily with oscillatory behavior at the applied RF. The RF field upon application initially heats up the electrons to about 0.03eV and as electrons begin escaping the system, the temperature quickly drops as the electrons with highest kinetic energy leave the system first and the slower electrons display a collective oscillation at the frequency of the RF field. Final temperature of our UCP system approaches a considerably low value which is promising from the perspective of ultra cold plasma.

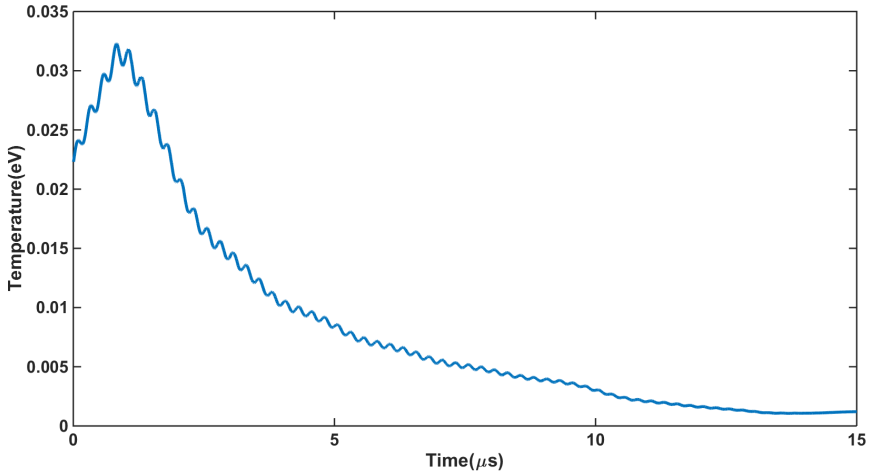

Figure 4.7: Temperature evolution of the UCP for density dependent resonant response

The potential at the center of the UCP system (Fig. 4.8) is the highest initially and begins to drop as the electrons start escaping the UCP. The now reduced electron density further drives the UCP expansion and the potential continues to drop with an oscillatory behavior at plasma frequency which is dependent on the density.

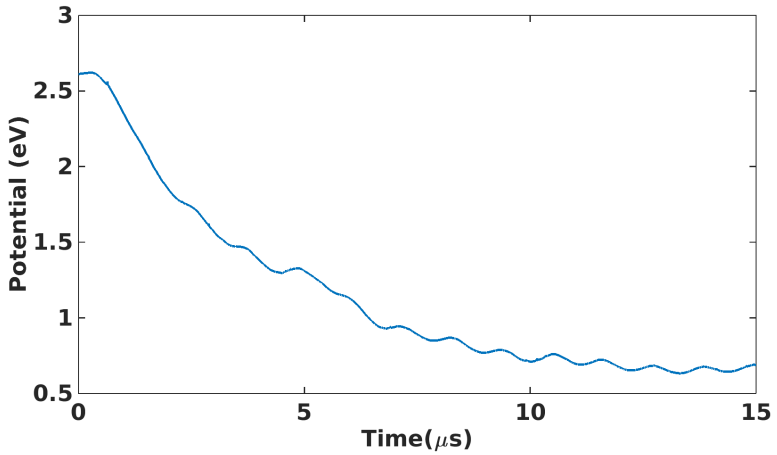

Figure 4.8: Potential at the center of the cube for the UCP density dependent resonant response

It is very important to consider collision processes in non-equilibrium plasma dynamics. Upon formation, the electrons and ions are not in thermal equilibrium with each other and as the UCP starts evolving the particles will work towards establishing a quasi-equilibrium.

The most important timescales for our system would involve electron-electron interactions or electron-ion interactions. For electron-electron interactions, the determination of time for a particle with $3/2k_BT$ of kinetic energy to undergo the same amount of energy changing collisions is the electron self-equilibration time given by,

$$t_{se} = \frac{0.266T_e^{3/2}}{n_e ln(\Lambda)} \tag{4.2}$$

where n_e is in cm^{-3} and T_e is in K. $\Lambda = 12\pi n_e \lambda_D^3$ where λ_D is the Debye screening length. For electron-ion collisions, we can find the time it would take for a net 90 degree deflection from an electron's original trajectory as

$$t_{90} = \frac{2\pi\epsilon_0^2\sqrt{me}(3K_BT)^{3/2}}{10^6 n_e e^4 ln(\Lambda)} \tag{4.3}$$

The electron-ion collision timescale also falls on the order of electron-electron collisions.

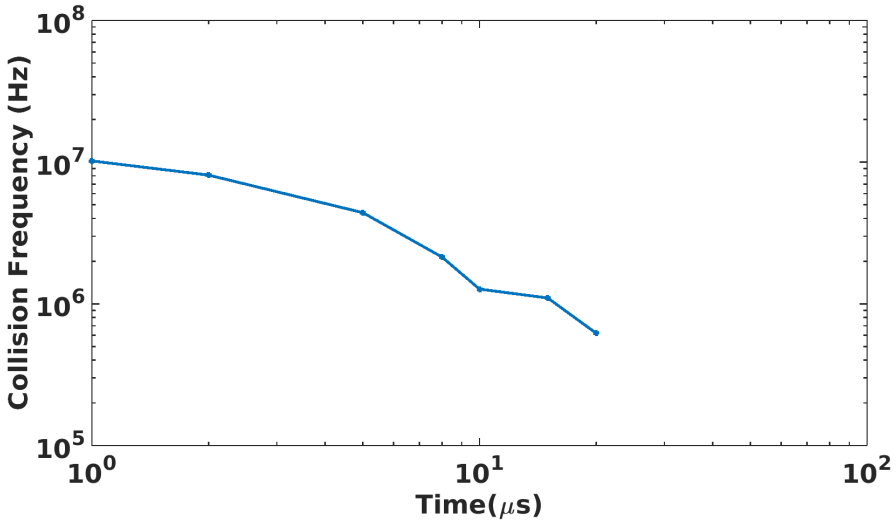

Figure 4.9: Coulomb collision frequency in the UCP over time for the simulation

For our UCP systems, these timescales range from tens of nanoseconds to a few microseconds according to the collision frequency calculated using the average density and estimated temperature, which will also allow us to study the physics of these ultracold plasmas in a regime where collisions are important and in a regime where we can treat the UCP as a collisionless fluid. However, UCPs have a non-uniform density and start with a uniform electron energy distribution. This complicates the exact meaning of these collision timescales, and are used as only estimates.

A direct comparison between continuous RF and the two cycle RF method cannot be made without accounting for heating of the UCP from the applied RF, which causes a shift in the resonance time. By accounting for the charge imbalance δ at the extrapolated time of resonance, we can determine the value of ω_{peak} which can give us a measure of the peak density n_{peak}. From this value of peak density and the total number of ions and electrons in our UCP N_{ion}, we can calculate the RMS size σ of a spherically symmetric gaussian distribution given by $\sigma = [N_{ion}/(2\pi)^{3/2} n_{peak}]^{1/3}$. This rms size can be used for an estimate of expansion of the UCP.

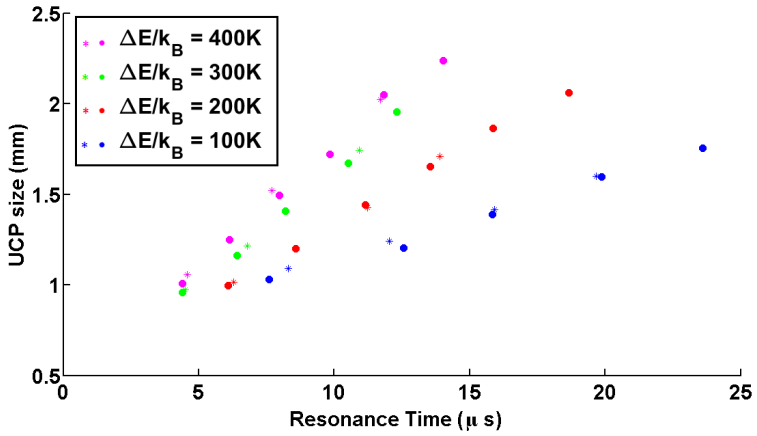

Figure 4.10: RMS size of the UCP for time of resonance for different frequencies of continuous RF ($*$) and two cycle RF ($\bullet$)

We plot the measured RMS size values using both the two cycle and continuous RF (Fig. 4.10) and there is no significant difference between the two techniques for values of $\Delta E/k_B$ ranging from 100K to 400K. We also measure the observed time of resonance as a function of the amplitude of the applied RF.

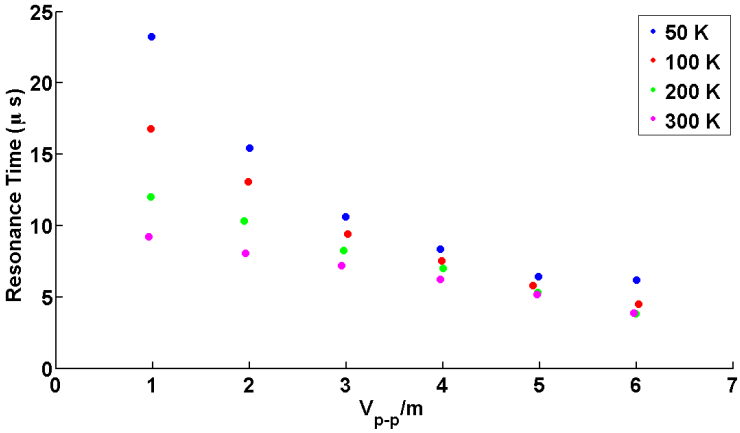

Figure 4.11: UCP resonance time variation with amplitude of RF field

From the above Fig. 4.11, it can be observed that for lower $\Delta E/k_B$ the peak time as a function of the applied RF amplitude is not linear. The extrapolation for higher energies however, is linear allowing us to make comparisons with two cycle method.

We observe that the electron and ion pair correlations (Fig. 4.12 and Fig. 4.13) are much weaker compared to the correlation functions obtained during early evolution of the ultra cold neutral plasma.

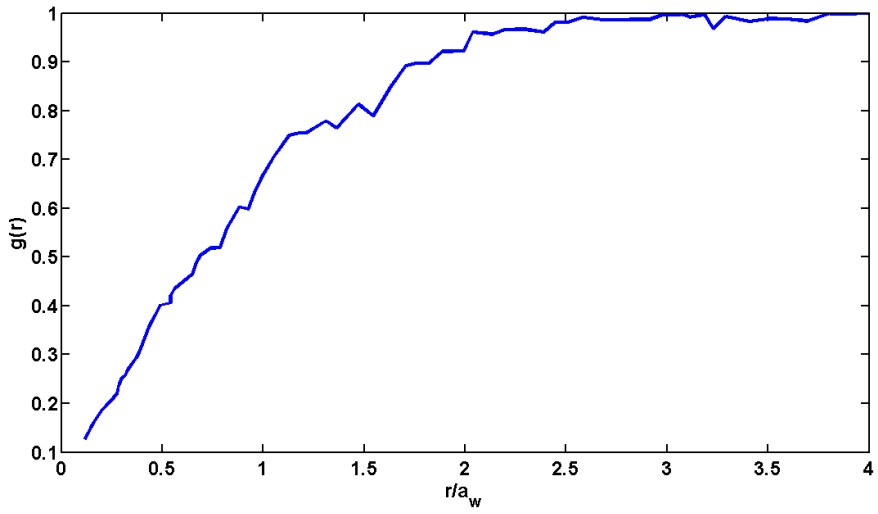

Figure 4.12: Electron pair correlation function at time of resonant response

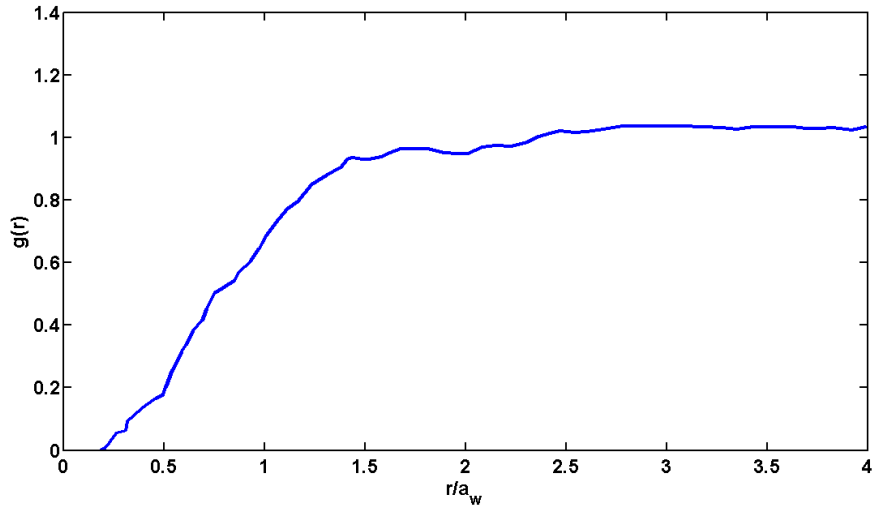

Figure 4.13: Ion pair correlation function at time of resonant response

This implies that the coupling, particularly in the electron component of the plasma has significantly weakened significantly, primarily due to the internal electric fields produced by the remaining charge densities, thus not allowing strong interactions between the two charged species.

Chapter 5

Conclusion And Future Work

The nature of response of the UCP to applied RF fields (continuous, delayed and short pulses) display a nearly collisionless mechanism for energy transfer within our low density UCP setup. The applied RF was shown to excite a collective oscillation of the electron cloud in the UCP with a resonant frequency. This collective response to the external fields show that this frequency can be determined by the peak density and charge imbalance in the plasma system. The methods used in these simulations allowed us to characterize different properties of the UCP. We achieve considerable qualitative agreement between our model with existing experiments for given initial conditions although we observe the correlation in the UCP weakens at the time of the density dependent resonant response denoting weaker coupling which maybe caused by the internal electric fields resulting in weaker interactions and possible three body recombination. We aim to explore fundamental physics of our system in collaboration with experimentalists and setting up a higher correlated gas. One of our goals is setting up a Fermi gas for higher correlations as opposed to the Rydberg gas where a higher density of atoms might be less likely. We could also use an adaptive Yukawa treecode model for comparison of Yukawa atoms with ion electron atoms and would like to set up our models as a virtual laboratory to help design experiment setups.

BIBLIOGRAPHY

BIBLIOGRAPHY

[1] T. C. Killian, S. Kulin, S. D. Bergeson, L. A. Orozco, C. Orzel, and S. L. Rolston, *Creation of an Ultracold Neutral Plasma*, Phys. Rev. Lett. 83, 4776 (1999)

[2] Truman Wilson, Wei-Ting Chen, Jacob Roberts, *Density-dependent response of an ultracold plasma to few-cycle radio-frequency pulses*, Phys. Rev. A. 87, 013410 (2013)

[3] Y.D. Jung, *Quantum-mechanical effects on electron - electron scattering in dense high-temperature plasmas*, Physics of Plasmas 8 (2001), 3842

[4] SG Brush, HL Sahlin, and E. Teller, *Monte carlo study of a one-component plasma. i*, The Journal of Chemical Physics 45 (1966), 2102

[5] S. Ichimaru, *Strongly coupled plasmas: high-density classical plasmas and degenerate electron liquids*, Reviews of Modern Physics 54, no. 4, 1017 (1982)

[6] GE Morfill, HM Thomas, U. Konopka, and M. Zuzic, *The plasma condensation: Liquid and crystalline plasmas*, Physics of Plasmas 6 , 1769-1780 (1999)

[7] AJ Christlieb, WNG Hitchon, JE Lawler, and GG Lister, *Integral and Lagrangian simulations of particle and radiation transport in plasma*, Journal of Physics D: Applied Physics 42, 194007 (2009)

[8] AJ Christlieb, R. Krasny, and JP Verboncoeur, *A treecode algorithm for simulating electron dynamics in a Penning-Malmberg trap*, Computer physics communications 164, no. 1-3, 306-310 (2004)

[9] AJ Christlieb, R. Krasny, and JP Verboncoeur, *Efficient particle simulation of a virtual cathode using a grid-free treecode Poisson solver*, IEEE Transactions on Plasma Science 32 , no. 2 (2004)

[10] AJ Christlieb, R. Krasny, and JP Verboncoeur,J.W. Emhoff, and I.D. Boyd *Grid-free plasma simulation techniques*, IEEE Transactions on Plasma Science 34 , no. 2, 149-165 (2006)

[11] G.B.Folland *Introduction to partial differential equations*, Princeton Univ Pr, 1995

[12] L.Greengard, *Fast algorithms for classical physics*, Science 265 (1994), no. 5174, 909

[13] J. Barnes and P. Hut, *A hierarchical 0 (N log N) force-calculation algorithm*, nature 324 , 4(1986)

[14] C.R. Anderson, *An implementation of the fast multipole method without multipoles*, SIAM Journal on Scientific and Statistical Computing 13, 923 (1992)

[15] L. van Dommelen and E.A. Rundensteiner, *Fast, adaptive summation of point forces in the two-dimensional Poisson equation*, Journal of Computational Physics 83, no. 1, 126-147 (1989)

[16] J.K. Salmon and M.S. Warren, *Skeletons from the treecode closet*, Journal of Computational Physics 111, no. 1, 136-155 (1994)

[17] W.D. Elliott and J.A. Board Jr, *Fast Fourier transform accelerated fast multipole algorithm*, SIAM Journal on Scientific Computing 17 , 398(1996)

[18] H. Cheng, L. Greengard, and V. Rokhlin *A fast adaptive multipole algorithm in three dimensions*, Journal of Computational Physics 155 , no. 2, 468-498 (1999)

[19] J. Makino, *Yet Another Fast Multipole Method without Multipoles-Pseudoparticle Multipole Method* 1*, Journal of Computational Physics 151 , no. 2, 910-920 (1999)

[20] W. Dehnen, *A hierarchical (n) force calculation algorithm*, Journal of Computational Physics 179, no. 1, 27-42 (2002)

[21] L. Ying, G. Biros, and D. Zorin, *A kernel-independent adaptive fast multipole algorithm in two and three dimensions* 1*, Journal of Computational Physics 196, no. 2, 591-626 (2004)

[22] S. G. Kuzmin and T. M. O'Neil, *Numerical Simulation of Ultracold Plasmas: How Rapid Intrinsic Heating Limits the Development of Correlation*, Phys. Rev. Lett. 88, 065003 (2002)

[23] S. D. Bergeson, A. Denning, M. Lyon, and F. Robicheaux, *Density and temperature scaling of disorder-induced heating in ultracold plasmas*, Phys.Rev. A 83, 023409 (2011)

[24] C. E. Simien, Y. C. Chen, P. Gupta, S. Laha, Y. N. Martinez, P. G. Mickelson, S. B. Nagel, and T. C. Killian, *Using Absorption Imaging to Study Ion Dynamics in an Ultracold Neutral Plasma*, Phys. Rev. Lett. 92, 143001 (2004)

[25] S. Kulin, T. C. Killian, S. D. Bergeson, and S. L. Rolston, *Plasma Oscillations and Expansion of an Ultracold Neutral Plasma*, Phys. Rev. Lett. 85, 318 (2000)

[26] K. A. Twedt and S. L. Rolston, *Electronic Detection of Collective Modes of an Ultracold Plasma*, Phys. Rev. Lett. 108, 065003 (2012)

[27] A. Lyubonko, T. Pohl, and J. M. Rost, *Collective energy absorption of ultracold plasmas through electronic edge-modes*, New J. Phys. 14, 053039 (2012)

[28] L. Spitzer, Jr. *Physics of Fully Ionized Gases*,(Dover, New York)(1962)

[29] Truman M. Wilson, *Dynamics of low-density ultracold plasmas in externally applied electric and magnetic fields*, Unpublished PhD thesis, Colorado State University (2013)

[30] G.B.Folland, *Introduction to Partial Differential Equations*, Princeton University Press (1995)

[31] Peijun Li, Hans Johnston, Robert Krasny, *A cartesian treecode for screened coulomb interactions*, Journal of Computational Physics 228, 3858-3868 (2009)

[32] P. Gupta, S. Laha, C. E. Simien, H. Gao, J. Castro, T. C. Killian, and T. Pohl, *Electron-Temperature Evolution in Expanding Ultracold Neutral Plasmas*, Phys. Rev. Lett. 99, 075005 (2007)

[33] T.C. Killian,T. Pattard, T. Pohl, J.M. Rost *Ultracold neutral plasmas*, Physics Reports 449, 77 ? 130 (2007)

[34] J.P.Verboncoeur *Particle simulation of plasmas : review and advances*, Plasma Physics and Controlled Fusion 47 (5A), A231 (2005)

[35] P. M. Bellan, *Fundamentals of Plasma Physics*, (Cambridge University Press, New York, 2006)

[36] D. A. Gurnett and A Bhattacharjee, *Introduction to Plasma Physics* (Cambridge University Press, 2005)

[37] S. Laha, P. Gupta, C. E. Simien, H. Gao, J. Castro, T. Pohl, and T. C. Killian, *Experimental Realization of an Exact Solution to the Vlasov Equations for an Expanding Plasma*, Phys. Rev. Lett. 99, 155001 (2007)

[38] H. J. Metcalf and P. van der Straten, *Laser Cooling and Trapping* (Springer-Verlag, New York, 1999)

[39] J.-H. Choi, B. Knuffman, X. H. Zhang, A. P. Povilus and G. Raithel, *Trapping and Evolution Dynamics of Ultracold Two-Component Plasmas*, Phys. Rev. Lett. 100, 175002 (2008)

[40] Michael E. Glinsky and Thomas M. O?Neil, *Guiding center atoms: Three-body recombination in a strongly magnetized plasma* , Phys. Fluids B 3 (5), (May 1991)

[41] F. Robicheaux and James D. Hanson, *Simulated expansion of an ultra-cold, neutral plasma*, Phys. Plasmas, Vol. 10, No. 6, (June 2003)

[42] M. Bonitz, D. Semkat, and D. Kremp, *Short-time dynamics of correlated many-particle systems: Molecular dynamics versus quantum kinetics*, Phys. Rev. E 56, 1246,(July 1997)